Geospace Storm Processes Coupling the Ring Current, Radiation Belt and Plasmasphere

M.-C. Fok[1], Y. Ebihara[2], T. E. Moore[1], D. M. Ober[3], and K. A. Keller[4]

The plasmasphere/ring-current/radiation-belt are interacting systems. The magnetic field generated by the ring current changes the drift paths of energetic particles. Pressure gradients in the ring current produce the region 2 field aligned currents, which close in the ionosphere and create an electric field that acts to shield the lower-latitude region from the full force of convection. In turn, this shielding field alters the transport of the ring current and plasmaspheric plasmas. Furthermore, the anisotropy in the ring current plasmas excites waves that cause pitch-angle and energy diffusion of radiation belt and ring current particles. On the other hand, the precipitation of energetic electrons modifies the ionospheric conductances, and thus the electric field configuration in the magnetosphere-ionosphere system. A number of models of the plasmasphere, ring current and the radiation belt have been developed to study the behaviors of the inner magnetosphere during geospace storms. However, the majority of these models are designed to study a particular plasma population, without the consideration of interactions from others. In this paper, we briefly describe state-of-the-art models of the plasmasphere, ring current, and radiation belt, and present results from a preliminary coupling effort. The coupled models are shown to produce certain observed features of the inner magnetosphere: the post-midnight peak of storm main phase ring current ion flux; the plasmaspheric disturbance produced by impulsive substorm plasma injections, and the slow ramp-up of geosynchronous fluxes associated with energy diffusion. We conclude by presenting a framework on coupling these models together interactively to make significant progress toward a realistic plasmasphere/ring-current/radiation-belt interaction model.

1. INTRODUCTION

The inner magnetosphere is commonly defined in the vicinity above the topside ionosphere at ~ 1000 km to L ~ 8. In the inner magnetosphere, the particle magnetic drifts are strong and depends on particle energy and pitch angle. As a result, charged particles with different energies and pitch angles drift differently and they cannot be described as a single fluid. There are three major plasma populations in the inner magnetosphere: the plasmasphere, the ring current and the radiation belt. The plasmasphere consists of cold (~ 1 eV) electrons and ions with density on the order of 1000 cm^{-3} inside the sharp boundary

[1] NASA Goddard Space Flight Center, Greenbelt, Maryland, USA
[2] National Institute of Polar Research, Tokyo, Japan
[3] Mission Research Corporation, New Hampshire, USA
[4] S P Systems, NASA Goddard Space Flight Center, Greenbelt, Maryland, USA

Inner Magnetosphere Interactions: New Perspectives from Imaging
Geophysical Monograph Series 159

10.1029/159GM16

called the plasmapause, whose location can vary from L ~ 2 to 6 depending on magnetic activities [*Carpenter and Anderson*, 1992]. The particle source of the plasmasphere is from the ionosphere. The shape of the plasmapause is controlled by convection, refilling rate from and loss rate to the ionosphere. The ring current is a population of hot electrons and ions with energies ranging from ~ 1 to 300 keV. It occupies from L~ 2 to 8 with particle density in the range of 0.1–10s cm^{-3}. Even though the ring current is much less dense than the plasmasphere, it carries most of the plasma pressure (~ 10–100 nPa) in the inner magnetosphere. The main particle source of the ring current is the plasma sheet, which consists of particles from the solar wind and the ionosphere. During geospace storms, particles are injected and accelerated from the plasma sheet into the ring current region. Strong convection force can push the ring current deeply inward to $L \leq 2$ on the nightside. During the main phases of storms, the ring current is highly asymmetric in local time with the peak located on the nightside [*Le et al*., 2004]. The ring current decays in the storm recovery and gradually becomes uniform in local-time. The radiation belt consists of relativistic electrons (E > 30 keV) and ions (E > 20 MeV). It occupies in the same region of the ring current. Radiation belt particles are originated in the solar wind, ionosphere and cosmic rays [*Walt*, 1996; *Baker et al*., 1996]. They can be accelerated and enhanced in intensity during various events and processes: solar energetic proton events, interplanetary shocks, storm sudden commencements, storm and substorm injections [*Baker et al*., 1996; *Hudson* et al., 1996; *Summers et al*., 1998; *Elkington et al*., 1999]. Though radiation belt particles contribute insignificantly in plasma density and pressure in the inner magnetosphere, their sources, sinks and variabilities are subjects of great interest because of the possible radiation hazards to spacecraft electronics and humans in space.

The plasmasphere, the ring current and the radiation belts are not independent populations. They interact with each other in many different ways. The plasmasphere provides the environment for various plasma wave generation and propagation. These waves may interact with the hot plasmas, causing diffusion, degradation and acceleration in energy and pitch angle of the energetic particles. Ring current ions experience energy degradation by interacting with the plasmaspheric electrons and ions through Coulomb collisions. *Fok et al*. [1991] found that Coulomb interactions are more important than charge exchange in determining the decay lifetimes for ring current H^+ below a few keV and for ring current He^+ and O^+ below a few tens of keV. On the other hand, the energy transferred to the plasmaspheric ions and electrons through Coulomb collisions with the ring current ions is a source of plasmasphere heating. *Fok et al.* [1993] calculated the energy deposition rate to the plasmasphere electrons and the corresponding heat flux to the subauroral ionosphere. The calculated heat flux is sufficient to produce a subauroral electron temperature enhancement and stable auroral red (SAR) arc emissions that are consistent with observations during active periods. The effects of ring current heating to the plasmasphere ions through Coulomb interactions were also investigated by *Fok et al.* [1995]. They calculated the plasmaspheric ion temperature with the additional heat flux from the ring current and reproduced the high ion temperatures often seen at high altitudes during storm times.

Energetic particles in the ring current often have anisotropic phase space distribution functions. When the effective ion temperature anisotropy $A = T_\perp / T_\parallel - 1$ exceeds some positive threshold, these particles will provide the free energy source needed to generate electromagnetic ion cyclotron (EMIC) waves [*Cornwall*, 1964, 1965; *Kennel and Petsheck*, 1966; *Lyons and Williams*, 1984]. In turn, the EMIC waves provide a mechanism to control the ring current evolution and precipitation loss rate [*Cornwall et al.,* 1971]. During the storm main phase, the ring current decay rate due to resonant interaction with EMIC waves can be substantially faster than the decay rate due to charge exchange or Coulomb scattering. *Fok et al.* [1993] and *Kozyra et al.* [1998] investigated the decay of the ring current ions using simple magnetic storm models considering loss mechanisms such as charge exchange and Coulomb collisions. They found additional loss processes, possibly wave-particle interactions, have to be included to account for the observed decay rates. Ring current particles also play important roles on the global convection in the inner magnetosphere and the subauroral ionosphere. A non-zero divergence in the ring current produces field aligned currents that flow out or into the ionosphere, where currents are closed through ionospheric currents [*Wolf*, 1983]. The resultant electric field generated in the ionosphere often opposes the original convection electric field and provides shielding of the inner magnetosphere from the full force of convection [*Wolf* 1995]. Another signature of the ring current is the self-generated magnetic field. During the main phase of a storm, the magnetic field produced by the ring current can significantly deplete the main field and alter the drift paths of plasmas, especially radiation belt particles. In order to conserve the third adiabatic invariant, energetic charged particles drift outward when the magnetic field is reduced. The particle energy thus decreases, and some of them may be lost from the trapped region if their drift paths encounter the magnetopause boundary. This is the

well-known Dst effect of the radiation belt that is often seen as a flux decrease during storm main phases [*Dessler and Karplus*, 1961; *Kim and Chan*, 1997].

Similar to the ring current ions, anisotropic pitch-angle distribution in energetic electrons (10–100 keV) excite whistler-mode waves in the magnetosphere [*Kennel and Petschek*, 1996; *Lyons et al*., 1972]. Wave-particle interactions play important roles on the development of radiation belt plasmas. *Lyons et al.* [1972] suggested that pitch-angle diffusion of radiation belt electrons resulting from resonant interactions with plasmaspheric whistler-mode waves (~ 300–1000 Hz) is responsible for the formation of the quiet-time electron slot region. *Summers and Ma* [2000] derived the energy spectra of relativistic electrons (> 1 MeV) in the inner magnetosphere by solving an energy diffusion equation, with the diffusion coefficient calculated based on gyroresonant electron-whistler mode wave interaction and parallel wave propagation. They found this stochastic acceleration of electrons is a viable mechanism for generating killer electrons during geomagnetic storms. This diffusive interaction is strong just outside the plasmapause, where the cold plasma density is low and the magnetic field strength is still relatively high [*Summers et al.,* 1998]. As the shape of the plasmasphere evolves during a storm, the region of strong energy diffusion will vary accordingly. This is another ample example of plasmasphere/radiation-belt coupling. Furthermore, energetic electrons have influences on the electric coupling in the global magnetosphere-ionosphere (M-I) system. Enhanced electron precipitations during geospace storms increase the ionospheric conductances and change the convection electric field, which, in turn, modifies the transport of the ring current and plasmasphere.

A number of physics-based models of the plasmasphere, ring current and the radiation belt have been developed to study the behavior of the inner magnetosphere during geospace storms [*Rasmussen et al*., 1993; *Ober et al*., 1997; *Chen et al*., 1994; *Fok and Moore*, 1997; *Fok et al*., 2001b, *Toffoletto et al*., 2003; *Jordanova et al.,* 1997; 2001, *Bourdarie et al*., 1996; 1997; *Fok et al.,* 2001a; *Zheng et al*., 2003]. However, the majority of these models are designed to study a particular plasma population, without the vigorous consideration of interactions from others. In this paper, we will briefly describe state-of-the-art models of the plasmasphere, ring current, and radiation belt. Only one model from each plasma population will be discussed as well as results from a preliminary coupling effort. We conclude by presenting a framework on coupling all these plasma populations together interactively to make significant progress toward a realistic plasmasphere/ring-current/radiation-belt interaction model.

2. STATE-OF-THE-ART MODELS OF THE INNER MAGNETOSPHERE

2.1 The Radiation Belt Environment (RBE) Model

The Radiation Belt Environment (RBE) model is a kinetic model that calculates the temporal variation of the phase space density of energetic electrons by solving the following bounce-averaged Boltzmann transport equation [*Fok et al*., 2001a; *Zheng et al*., 2003]:

$$\frac{\partial f_s}{\partial t}+\left\langle \dot{\lambda}_i \right\rangle \frac{\partial f_s}{\partial \lambda_i}+\left\langle \dot{\phi}_i \right\rangle \frac{\partial f_s}{\partial \phi_i}=\frac{1}{\sqrt{M}}\frac{\partial}{\partial M}\left(\sqrt{M}\,D_{MM}\,\frac{\partial f_s}{\partial M}\right) + \frac{1}{T(y)\sin 2\alpha_o}\frac{\partial}{\partial \alpha_o}\left(T(y)\sin 2\alpha_o D_{\alpha_o\alpha_o}\frac{\partial f_s}{\partial \alpha_o}\right)-\left(\frac{f_s}{0.5\tau_b}\right)_{\text{loss cone}} \quad (1)$$

where $f_s = f_s\left(t,\lambda_i,\phi_i,M,K\right)$, is the average distribution function on the field line between mirror points. λ_i and ϕ_i are the magnetic latitude and local time, respectively, at the ionosphere foot point of the geomagnetic field line. M is the relativistic magnetic moment and $K = J/\sqrt{8m_o M}$, where J is the second adiabatic invariant. The motion of the particles is described by their drifts across field lines which are labeled by their ionospheric foot points. The M range is chosen to well-represent the energy ranges of electrons from 10 keV to 4 MeV. The K range is chosen to cover the loss cone so that particle precipitations can be estimated as well.

The left hand side of (1) represents the drifts of the particle population and the terms on the right hand side of (1) refer to diffusion and loss. The calculation of the bounce-averaged drift velocities, $<\lambda i>$ and $<\phi i>$, were described in detail in *Fok and Moore* [1997]. These drifts include gradient and curvature drift, and EXB drift from convection and corotation electric fields. The effects of inductive electric field due to time-varying magnetic field are also taken into account implicitly in the model. For this purpose, we have assumed that field lines are rooted at the ionosphere, so that the inductive electric field there is zero. However, the shapes of field lines at higher altitudes vary as a function of time according to the magnetic field model. If field lines are perfect conductors, the field line motion at high altitudes, e.g., at the equator, will generate an induction electric field of the form,

$$\mathbf{E}_{\text{ind}} = -\,\mathbf{v}_o \times \mathbf{B}_o \quad (2)$$

where $\mathbf{v}_o$ and $\mathbf{B}_o$ are the field line velocity and magnetic field at the equator.

The first term on the right hand side of (1) represents particle diffusion in M as a result of energy diffusion due

to interactions with plasma waves. The relation between energy diffusion coefficient (D_{EE}) and the corresponding coefficient in M (D_{MM}) is given as,

$$D_{MM} = D_{EE}\left(\frac{\partial M}{\partial E}\right)^2 = D_{EE}\left(\frac{E_o + E}{E_o B_m}\right)^2 \qquad (3)$$

where E_o is the electron rest energy and B_m is the magnetic field at the mirror point. The second term on the right hand side of (1) represents pitch-angle diffusion from interacting with waves, where α_o is the equatorial pitch angle. For pure pitch-angle diffusion (E unchanged) in the (M, K) coordinates, we first map the particle phase space density from the (M, K) to (E, α_o) coordinates, perform diffusion in α_o, and then map the updated distribution back to the (M, K) coordinates [*Fok et al.,* 1996]. The diffusion terms are followed by the loss term of the loss cone, the boundary of which is assumed to correspond to mirror height of 120 km. Particles in the loss cone are assumed to have a lifetime of one half bounce period ($0.5\,\tau_b$).

Eq. (1) includes multiple terms of different processes. We use the method of fractional step to decompose the equation and solve only one term at a fractional step [*Fok et al*., 1993]. To solve (1), we have to specify the electric, magnetic fields and the particle distribution on the nightside boundary, which is set at 10 Earth radii (R_E). We have been using empirical models such as Tsyganenko 1996 model [*Tsyganenko* 1995] for the magnetic field and Weimer model [*Weimer* 2001] for electric field [*Zheng et al.,* 2003]. We have also run the RBE model with the magnetic and electric fields output from the Block-Adaptive-Tree-Solarwind-Roe-Upwind-Scheme (batsrus) MHD model [*Groth et al.,* 2000; *Gombosi et al.,* 2003]. Both the electric and magnetic fields are updated every 5 minutes or less. The effect of radial diffusion is integrated in these time-varying fields.

The RBE model is almost the unique existing model that provides predictions of energetic electron distributions covering the entire radiation belt region and energy, with the considering of realistic and time-varying magnetic and electric fields. *Zheng et al*. [2003] showed that the RBE model gives reasonably well agreements with the observed energetic (50 keV–1.5 MeV) electron fluxes at the geosynchronous orbit. The model-data agreements are better when time-varying magnetic field was employed, indicating the importance of magnetic field configuration in controlling the transport of radiation belt particles.

2.2 The Comprehensive Ring Current Model (CRCM)

The Comprehensive Ring Current Model (CRCM) combines the Rice Convection Model (RCM) [*Harel et al*., 1981] and the Fok ring current model [*Fok et al*., 2001b]. The Fok ring current is similar to the RBE model described above, except the M range is chosen to cover the ring current energy (~ 1–300 keV) and charge exchange loss is also included. To couple with the Fok model, the RCM algorithm for calculating Birkeland currents has been generalized to arbitrary pitch angle distribution [*Fok et al*., 2001b]. Plate 1 shows the model logic of the CRCM. Given an initial ring current distribution (f_s), the RCM component of the CRCM computes the ionospheric electric current:

$$J_{\|i} = \frac{B_i}{B}\sum_j \mathbf{b}\bullet\nabla\eta_j \times \nabla E_j \qquad (4)$$

where $J_{\|i}$ is the current per unit area parallel to $\mathbf{B}_i$; positive current is down into the ionosphere, B_i is the magnetic field strength in the ionosphere, η_j is the number of particles of type j per unit magnetic flux in the range $\Delta M \Delta K$, and E_j is the kinetic energy. The η_j associated with a range $\Delta M \Delta K$ is related to the distribution function, f_s, by [*Fok et al*., 2001b]:

$$\eta_j = f_s 4\sqrt{2}\pi\, m_o^{3/2} M_j^{1/2} \Delta M_j \Delta K_j \qquad (5)$$

The summation in (4) sums all the contributions from different particle type (M and K) to the field aligned current. Given a specification of ionospheric conductance, the ionospheric potential, Φ, is calculated by solving

$$\nabla\bullet\left(-\ddot{\Sigma}\bullet\nabla\Phi\right) = J_{\|i}\sin I \qquad (6)$$

where $\ddot{\Sigma}$ is a conductance tensor, and I is the magnetic dip angle. The Fok model then advances the plasma distribution using the electric field computed by (6) and at the same time calculates particle losses along drift paths. The updated distributions are then returned to the RCM to complete the computation cycle.

Input models required for running the CRCM include a magnetic field model, the electric potential at high-latitude ionosphere boundary (near the polar cap), an ionospheric conductance model, and the plasma sheet distribution function at the equator at the CRCM outer boundary. Currently the Tsyganenko 1996 model [*Tsyganenko* 1995] is used for the magnetic field configuration. The electric potential at the polar boundary is modeled by the Weimer 2000 model [*Weimer* 2001] or by the Boyle model [*Boyle et al.,* 1997]. The CRCM conductance model superimposes a *Hardy et al.* [1987] auroral enhancement on a background conductance based on the MSIS neutral atmosphere [*Hedin,* 1991], the IRI-90 ionospheric model [*Bilitza et al*., 1993], and collision-frequency expressions given by *Riley* [1994]. The plasma sheet distribution at 10 R_E is assumed to be a Maxwellian

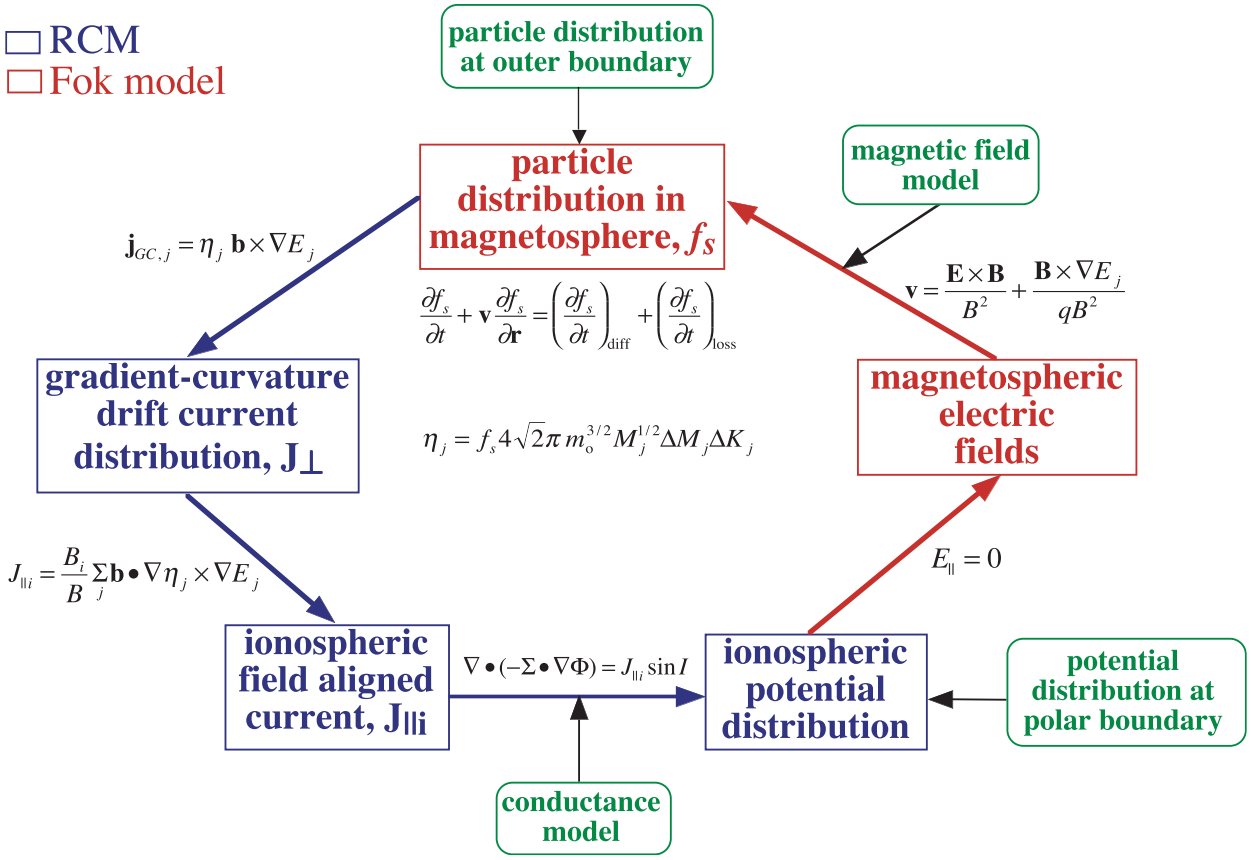

Plate 1. The model logic of the Comprehensive Ring Current Model. Blue boxes are the Rice Convection Model, red boxes the Fok model, and green boxes input models.

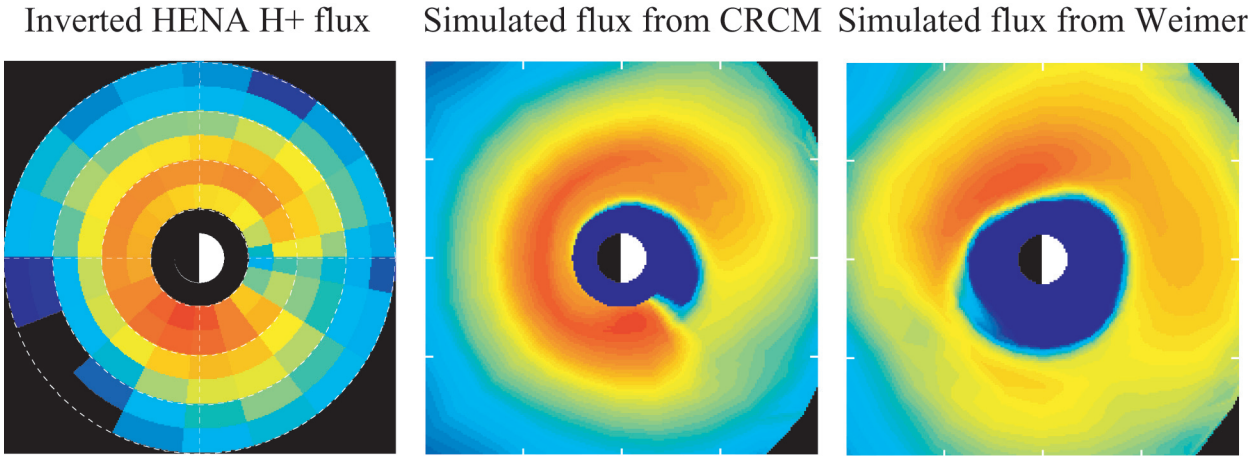

Plate 2. Left panel: equatorial flux of 32 keV H^+ inverted from the HENA image at 09:00 UT on 12 August 2000. Middle panel: simulated flux at the same energy and time calculated by the CRCM. Right panel: simulated flux using the Weimer electric field model.

with constant density of 0.5 cm^{-3} and temperature 5 keV. In some studies, we varied the boundary temperature and density according to the upstream solar wind conditions [*Fok et al*., 2003].

The CRCM is the first ring current model that self-consistently solves the magnetospheric plasma distribution and ionospheric current and potential, with the consideration of arbitrary pitch-angle distribution in the ring current plasmas. The CRCM has been very successful in reproducing observable features of the storm-time ring current. In modeling the storm on 2 May 1986, near the peak of the storm when convection was strong, the model developed a region of strong outward electric field at $L \sim 3$ in the dusk-midnight sector [*Fok et al*., 2001b]. This appears to be the same feature that was noted by *Rowland and Wygant* [1998] and *Burke et al.* [1998] in CRRES electric data for major storms. In the ionosphere, this signature corresponds to a strong poleward field in the subauroral region that has very similar characteristics as the subauroral polarization stream (SAPS) identified by *Foster and Vo* [2002]. The CRCM also reproduced and provided possible explanations to the post-midnight enhancements in storm-time ring current seen by the High Energy Neutral Atom (HENA) imager on the Imager for Magnetopause-to-Aurora Global Exploration (IMAGE) mission [*C:son Brandt et al*., 2002]. *Fok et al*. [2003] found that the post-midnight peak is a combined effect of the irregularities in the ionosphere conductance and the strong shielding field generated by the ring current ions. Plate 2 shows the equatorial flux of 32 keV H^+ inverted from the HENA image [*Roelof and Skinner*, 2000] at 09:00 UT on 12 August 2000 (left panel), showing a flux maximum near dawn. The middle panel plots the simulated flux at the same energy and time calculated by the CRCM. It can be seen that the CRCM produces a very similar local-time distribution. In contrast, the simulation using the empirical electric field model of *Weimer* [1995] gives the peak flux at the dusk-midnight sector (right panel). This comparison strongly illustrates the superiority of self-consistent electric field over empirical models.

2.3 Dynamic Global Core Plasma Model (DGCPM)

A Dynamic Global Core Plasma Model (DGCPM) has been developed to calculate the plasma flux tube contents and equatorial plasma density distribution versus time throughout the magnetosphere, including the influences of convection on the flux tube volumes, as well as daytime refilling and nighttime draining of plasma [*Ober et al*., 1997]. The model solves the following continuity equation of the total ion content of a magnetic flux tube:

$$\frac{D_{\perp} N}{Dt} = \frac{F_N + F_S}{B_i} \tag{7}$$

where D/Dt is the convective derivative in the ExB frame of the flux tube, N is the total ion content per unit magnetic flux, F_N and F_S are the ionospheric fluxes in or out of the flux tube at northern and southern ionospheres, and B_i is the magnetic field at the ionospheric foot points of the flux tube. The equatorial plasma density is assumed to be equal to the average density in the flux tube.

The net flux of plasmas in or out of a flux tube depends on the instantaneous content of the flux tube. The particle flux on the dayside, F_d, is given by:

$$F_d = \frac{n_{sat} - n}{n_{sat}} F_{max} \tag{8}$$

where n_{sat} is the saturation density [*Carpenter and Anderson*, 1992], n is the plasma density in the flux tube, and F_{max} is the limiting flux from the ionosphere [*Chen and Wolf*, 1972]. The nightside flux, F_n, is approximated by:

$$F_n = -\frac{N\, B_i}{\tau} \tag{9}$$

where τ is the downward diffusion lifetime on the nightside, which is assumed to be 10 days.

Observable features in the plasmasphere are reproduced by the DGCPM. A subauroral ion drift (SAID) event was modeled by the DGCPM [*Ober et al*., 1997]. They found that imposing a SAID event in the dusk-evening sector of 30 minutes leads to the formation of a narrow embedded plasma density troughs generally resemble plasmasphere density profiles observed from DE 1 measurements. The DGCPM has the feasibility to allow user provided convection field and magnetic field (flux tube volume), and is thus easy to couple with other models.

3. PRELIMINARY RESULTS ON MODEL COUPLING

We have started coupling the DGCPM, CRCM, and RBE in various ways. We have incorporated the DGCPM inside the CRCM, driving the plasmasphere model with the electric field output from the CRCM. The storm on 17 April 2002 is studied. At 10:20 UT on 17 April 2002, an interplanetary shock was recorded by the Advanced Composition Explorer (ACE) satellite. About 50 minutes later at ~ 11:10 UT, the shock arrived at the Earth, strongly compressed the dayside magnetopause and produced a sharp jump in the symH index. A magnetic storm commenced after the compression and symH attained a value of –90 nT at ~19:00 UT. From 19:00–20:40 UT, IMAGE was ascending from the apogee. The EUV imager [*Sandel et al*., 2000] on IMAGE captured clear images of the plasmasphere during this period of time.

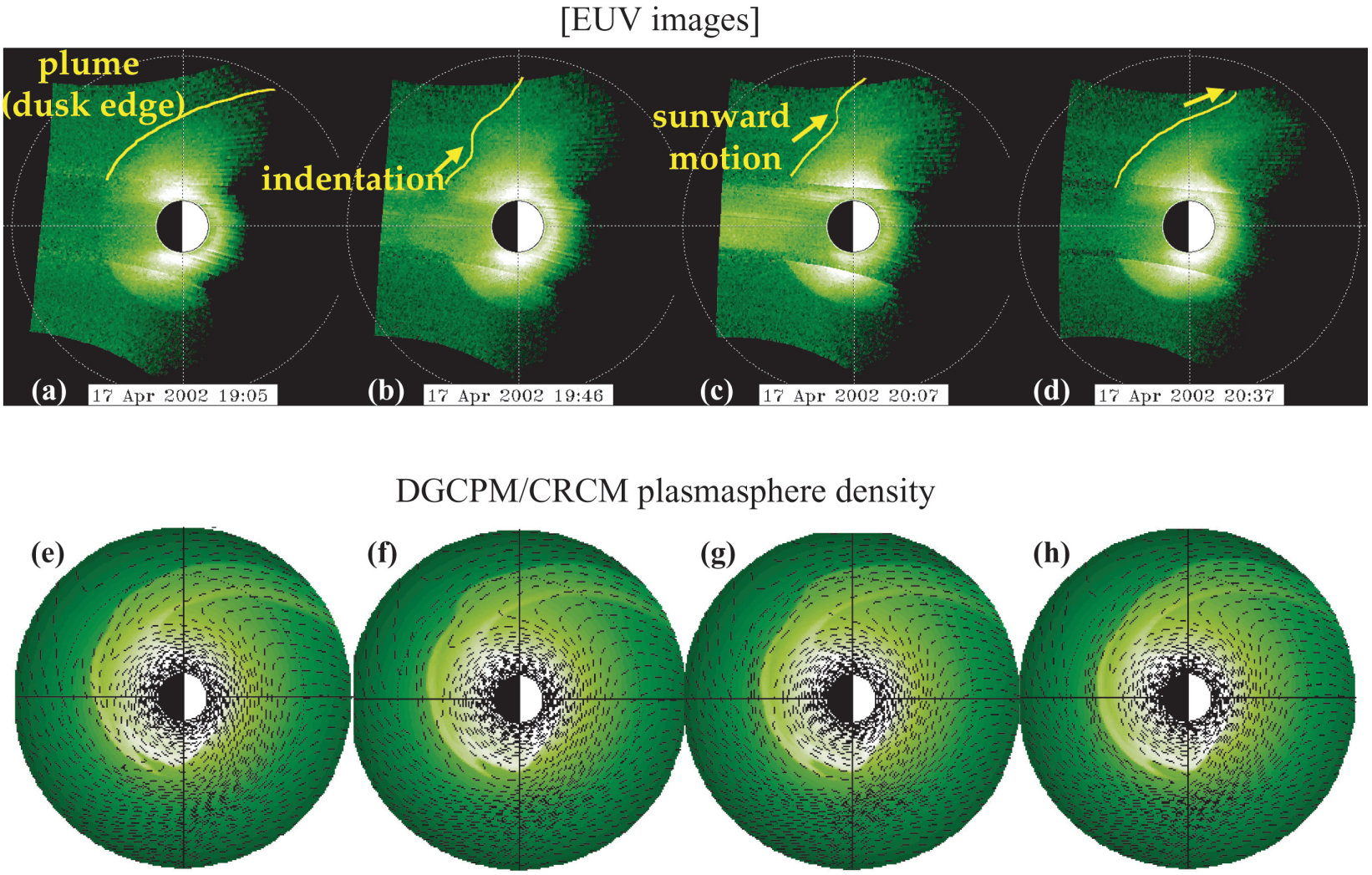

Plate 3. Top panels: plasmasphere undulation seen by IMAGE/EUV imager from 19:05–20:37 UT on 17 April 2002. Bottom panels: DGCPM/CRCM simulated images of the undulation event.

The upper panels of Plate 3 show four EUV images from 19:05–20:37 UT. The dim area on the nightside is the shadow of the Earth. As shown in Plate 3a, a plasma plume was seen on the dusk-side at 19:05 UT. At this moment, a substorm onset was detected by the IMAGE/FUV SI13 aurora images and IMAGE/HENA saw ring current injection after the onset (Jerry Goldstien, private communication). At 19:46 UT, an indentation of the plasmapause was seen in the EUV image (Plate 3b). This notch feature then moved westward to the dayside in the following hour and disappeared at ~ 20:37 UT (Plate 3c, d).

The lower panels of Plate 3 display the calculated plasmasphere density by the DGCPM, which drives the flux tube motion by the CRCM electric field. The black dashed lines are convection potential contours with co-rotation. As shown in Plate 3e–h, the combined DGCPM/CRCM reproduces the plasmasphere undulation seen by IMAGE/EUV data. By comparing the calculated electric potentials during and prior the undulation event, we found that the model predicts a strong shielding field produced by ring current injection during the undulation. The weak convection field at the plasmapause at 18–21 MLT causes outward motion or undulation of the plasmapause at this local time region (Plate 3f). The notch is then striped westward by the stronger convection later in time (Plate 3g–h). This scenario is consistent with the HENA data, which detect a substorm injection and enhanced ring current pressure during the plasmasphere undulation at ~ 19–20 UT. The field aligned current generated from the freshly injected ring current ions shields (or even over-shields) the plasmasphere region from the convection field and produces this wavy structure of the plasmasphere. *Liemohn et al.* [2004] simulated the plasmasphere shape during this storm using three electric field models: the McIlwain analytical model, the Weimer statistical model, and a self-consistent model. They also found the self-consistent model is the best in reproducing the plasmapause locations observed by the IMAGE/EUV data.

An accurate specification of the plasmasphere is necessary in order to precisely calculate the pitch-angle and energy diffusion of radiation belt particles due to wave-particle interactions. We have also integrated the DGCPM with the RBE model, driving both the transport of the plasmasphere and radiation belt plasmas with the same electric and magnetic fields. We have used the combined DGCPM/RBE model to simulate the energetic electron fluxes during the space storm on May 2–6, 1998. A coronal mass injection (CME) and magnetic cloud were observed by the ACE satellite on May 2–4. At the end of the CME on May 4, a high-speed stream was observed with large increases in solar wind speed, temperature and magnetic field [*Skoug et al*., 1999]. This stream hit the magnetosphere on early May 4 and triggered a geospace storm with a minimum Dst of –200 nT. The recovery phase was long and jagged as seen in the Dst index.

We calculated the energetic electron fluxes on May 2–6, 1998 using the RBE model with the electric and magnetic fields output from the batsrus MHD model. The magnetic and electric field is updated every 4 minutes. The plasma sheet distribution at the nightside boundary of the RBE model at 10 R_E is assumed to be a kappa function with density (N_{ps}) and characteristic energy (E_{ps}) modeled by linear relations with the upstream solar wind conditions [*Zheng et al*., 2003]:

$$\begin{aligned} N_{ps}(t) &= [0.02 * N_{sw}(t-3\text{hr}) + 0.316] * \sqrt{\text{amu}} \\ E_{ps}(t) &= 0.016 * V_{sw}(t-3\text{hr}) - 2.4 \end{aligned} \tag{10}$$

where N_{ps} is in cm^{-3}, N_{sw} is the solar wind density in the same unit, amu is the atomic mass unit of electron, E_{ps} is in keV, and V_{sw} is solar wind velocity in km s^{-1}. Note that there is a 3-hour time lag between the plasma sheet condition and solar wind condition at the dayside magnetopause.

We have performed two model runs for this event. In the first one we consider particle drift and loss-cone loss only. In the second run, we include the effect of energy diffusion due to interacting with the whistler mode waves. *Summers and Ma* [2000] have derived a simple expression for the energy diffusion coefficient based on gyroresonant electron-whistler mode wave interaction and parallel wave propagation. They expressed the energy diffusion coefficient, D_{EE}, as:

$$\begin{aligned} D_{EE} &= D_{\text{o}}[E_n(E_n+2)]^{1/2} / (E_n+1) \\ D_{\text{o}} &= \frac{\pi(\gamma-1)}{8} \frac{e}{\sqrt{m_p}} \left(\frac{\Delta B\, B_{\text{o}}}{m_e} \right)^2 \left(\frac{\varepsilon_{\text{o}}}{n_e} \right)^{1.5} \end{aligned} \tag{11}$$

where E_n is electron kinetic energy normalized by electron rest mass energy, γ is the turbulence spectral index which is assumed to equal to 5/3, ΔB is the whistler amplitude, B_{o} is the magnetic field at the equator, n_e is the plasmasphere density, and the rest of the symbols represent their commonly used definitions. In order for electrons to resonate with whistler waves, the kinetic energy of the electron must exceed a critical value [*Summers and Ma*, 2000]:

$$E_n \geq E_c = \left(1 + \frac{m_p \text{v}_A^2}{m_e c^2} \right)^{1/2} - 1 \tag{12}$$

where E_c is the normalized critical energy and v_A is the Alfven speed. As shown in (11), strong energy diffusion

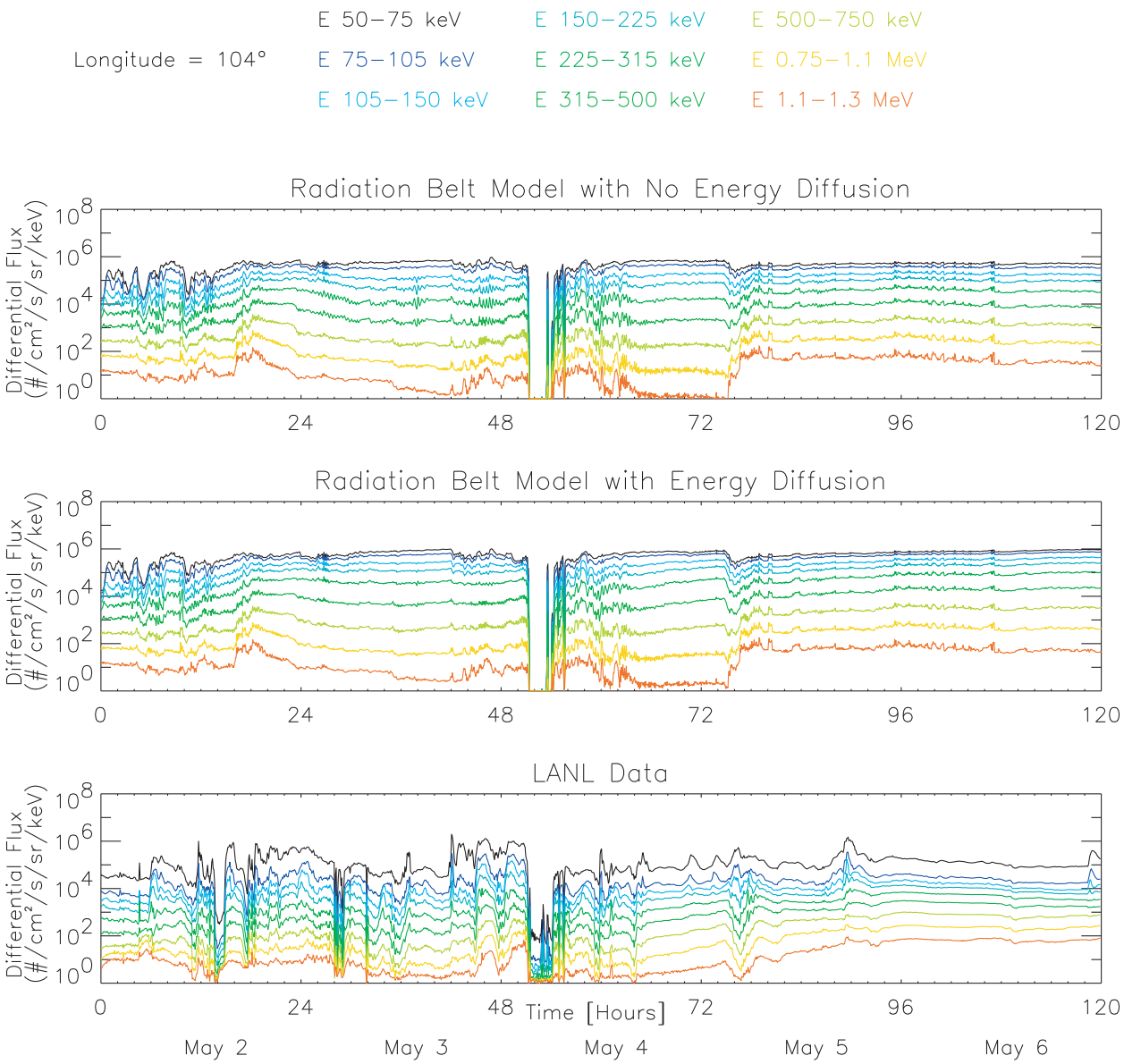

Plate 4. Top panel: simulated geosynchronous electron fluxes at 104˚ longitude on May 2-7, 1998, without energy diffusion. Middle panel: same as the top panel except with energy diffusion. Bottom panel: energetic electron data from LANL satellite 1994-084.

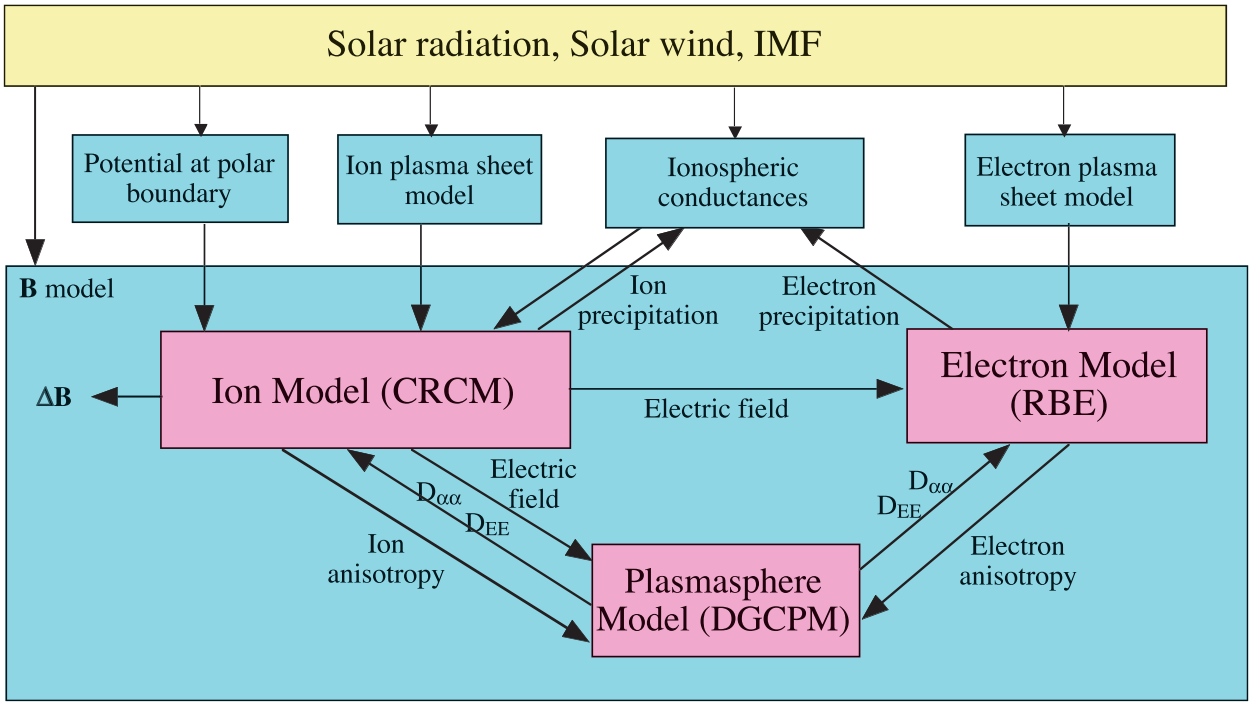

Plate 5. The model logic of the plasmasphere/ring-current/radiation-belt interaction model (PRRIM).

happens just outside the plasmapause, where B_0 is strong and n_e is low. While the shape of the plasmasphere is changing during a storm, the region of strong energy diffusion varies accordingly. We calculate the energy diffusion coefficient using (11) with n_e given by the DGCPM imbedded in the RBE model. The whistler wave amplitude (ΔB) is assumed to be a constant of 50 pT throughout the storm.

Plate 4 shows the simulated and observed electron differential fluxes at energies from 50 keV to 1.3 MeV at the geosynchronous orbit at the longitude of the Los Alamos National Laboratory (LANL) satellite 1994-084. The top and middle panels are calculated electron fluxes without and with energy diffusion, respectively. The LANL Synchronous Orbit Particle Analyzer (SOPA) data are plotted in the bottom panel. As shown in the figure, the calculated fluxes generally agree well with the LANL data. The sharp flux drop out at 04:00–06:00 UT on May 4 is seen in both the observed and calculated data. This flux decrease is due to the incursion of the dayside magnetopause inside the geosynchronous orbit. The batsrus MHD model is able to reproduce the shape of this severely-compressed magnetosphere. During the recovery phase of the storm from late May 4 to May 7, the observed fluxes with energies $\geq$ 300 keV slowly increased except at 04:00–06:00 UT on May 5. The simulated fluxes show a jump also at 04:00–06:00 UT on May 5 when the interplanetary magnetic field (IMF) was turning northward (Plate 4, top two panels). However, other than this fluctuation, the calculated fluxes are pretty steady during the storm recovery. With the inclusion of energy diffusion (middle panel), the calculated fluxes are higher than those without energy diffusion and agree better with the LANL data. In particular, on late May 4 to early May 5, the calculated electron distributions with energy diffusion show a slow increase in fluxes, consistent with the LANL data.

4. A PLASMASPHERE/RING-CURRENT/RADIATION-BELT INTERACTION MODEL

The simulation results from coupling the ionosphere-magnetosphere and hot-cold plasmas presented in the previous sections are very encouraging. However, there is still much room for improvement. The CRCM ion flux shown in Plate 2 is calculated using an empirical model of the height integrated ionospheric conductance. *Khazanov et al*. [2003a] calculated the ionosphere conductance according to the precipitated energetic electron and ion fluxes output from their self-consistent ring current model during the storm on 2 May 1986. They found deeper penetration of the convection electric field when conductances were calculated self-consistently. In order to estimate the effects of energy diffusion on radiation belt enhancement, we have applied a constant wave amplitude. In fact, it is well known that the rate of wave growth and thus wave amplitude depends on the temperature anisotropy of energetic electrons and ions [e.g., *Kennel and Petsheck*, 1966].

Plate 5 presents our design of a comprehensive plasmasphere/ring-current/radiation-belt interaction model (PRRIM). Many of the important processes linking the ionosphere, ring current, plasmasphere and radiation belt are included. In PRRIM, the geospace system is solely driven by the solar wind, IMF and solar radiation. The magnetic field model, cross polar cap potential, ion and electron plasma sheet distributions are determined by the IMF, solar wind density and temperature in the subsolar region. The background conductance varies with the solar F10.7 flux. The simulated ion and electron precipitations from the CRCM and RBE model are utilized to calculate the auroral conductance. The energy and pitch-angle diffusion of energetic ions and electrons are computed consistent with the ion and electron anisotropies [*Jordanova et al*., 2001; *Khazanov et al*., 2003b; *Horne et al*., 2003], in the core plasma environment given by the DGCPM.

The CRCM, RBE and DGCPM are driven by the same magnetic field model and the electric field output from the CRCM. In the recent Tsyganenko models [*Tsyganenko* 1995; 2002], Dst is used to model the strength of the symmetric and partial ring current. We propose a more self-consistent way to simulate the ring current effect on the global magnetic configuration, that is to modify the symmetric and partial components of the ring current in Tsyganenko models by the actual ion currents calculated in the CRCM. In the case of MHD provided magnetic and electric fields, implementing the ring current contribution to the magnetic field would not be so straight forward. However, better description of the subauroral electric field can be obtained by replacing the MHD electric field by the field output from the CRCM. The MHD model only provides the potential at the CRCM high-latitude boundary.

5. DISCUSSIONS AND SUMMARY

The main purpose of this paper is to present our design of a plasmasphere/ring-current/radiation-belt interaction model. With all the components having been developed in certain degree of maturity, it is timely to couple and integrate these models together interactively. The PRRIM outlined in Plate 5 does not represent a perfect and fully completed model of the inner magnetosphere. One obvious weakness of the PRRIM is its crude or lack of self-consistency in handling the magnetic field. A vigorous way to treat the magnetic coupling self-consistently requires a large amount of computer time and careful schemes to assure numerical stability [*DeZeeuw*

et al., 2001; *Gombosi et al*., 2003]. We have chosen a simple approach (modifying the ring current component in Tsyganenko models) to implement the effect of ring current on the magnetic field because we aim to develop a precise but efficient model of the inner magnetosphere. The scheme presented in Plate 5 already represents a major progress in modeling the M-I system. In summary, we have

(1) given brief descriptions of three state-of-the-art models of the ring current (CRCM), radiation belt (RBE) and plasmasphere (DGCPM).

(2) Coupling results of these models produce certain observed features of the inner magnetosphere: the post-midnight peak of storm main phase ring current ion flux; the plasmaspheric disturbance produced by substorm plasma injections, and the slow ramp-up of geosynchronous fluxes associated with energy diffusion.

(3) We have outlined a framework on coupling these models interactively to develop a comprehensive plasmasphere/ring-current/radiation-belt interaction model.

Acknowledgments. We thank Richard Wolf for many insightful discussions. The IMAGE/EUV data are provided by Jerry Goldstein and LANL/SPOA data by Geoff Reeves. The MHD output for the May 1998 event is provided by the Community Coordinated Modeling Center. This work is supported by the NASA Office of Space Science Sun-Earth Connection Guest Investigator Program under RTOP Grant 370-16-00-11 and IMAGE mission under UPN 370-28-12.

REFERENCES

Baker, D. N., S. G. Kanekal, M. D. Looper, J. B. Blake, and R. A. Mewaldt, Jovian, Solar, and other possible sources of radiation belt particles, in *Radiation Belts: Models and Standards, Geophys. Monogr. Ser.,* vol. 97, edited by J. F. Lemaire et al., pp. 49–55, AGU, Washington, D. C., 1996.

Bilitza, D., K. Rawer, L. Bossy, and T. Gulyaeva, International reference ionosphere–Past, present, future, *Adv. Space Res., 13*(3), 3–23, 1993.

Bourdarie, S., D. Boscher, T. Beutier, and J. Sauvaud, Magnetic storm modeling in the Earth's electron belt by the Salammbô code, *J. Geophys. Res.*, *101*, 27,171–27,176, 1996.

Bourdarie, S., D. Boscher, T. Beutier, J.-A. Sauvaud, and M. Blanc, Electron and proton radiation belt dynamic simulations during storm periods: A new asymmetric convection-diffusion model, *J. Geophys. Res., 102*, 17,541–17,552, 1997.

Boyle, C. B., P. H. Reiff, and M. R. Hairston, Empirical polar cap potential, *J. Geophys. Res., 102*, 111–125, 1997.

Burke, W. J., N. C. Maynard, M. P. Hagan, R. A. Wolf, G. R. Wilson, L. C. Gentile, M. S. Gussenhoven, C. Y. Huang, T. W. Garner, and F. J. Rich, Electrodynamics of the inner magnetosphere observed in the dusk sector by CRRES and DMSP during the magnetic storm of June 4–6, 1991, *J. Geophys. Res.*, *103*, 29,399–29,418, 1998.

Carpenter, D. L. and R. R. Anderson, An ISEE/whistler model of equatorial electron density in the magnetosphere, *J. Geophys. Res., 97*, 1097–1108, 1992.

Chen, A. J., and R. A. Wolf, Effects on the plasmasphere of a time-varying convection electric field, *Plant. Space Sci., 20*, 483–509, 1972.

Chen, M. W., L. R. Lyons, and M. Schulz, Simulations of phase space distributions of storm time proton ring current, *J. Geophys. Res., 99*, 5745–5759, 1994.

Cornwall, J. M., Cyclotron instabilities and electromagnetic emission generation, *J. Geophys. Res., 69*, 4515, 1964.

Cornwall, J. M., Cyclotron instabilities and electromagnetic emission in the ultra low frequency and very low frequency ranges, *J. Geophys. Res., 70*, 61, 1965.

Cornwall, J. M., F. V. Coroniti, and R. M. Thorne, Unified theory of SAR arc formation at the plasmapause, *J. Geophys. Res., 76*, 4428, 1971.

C:son Brandt, P., S. Ohtani, D. G. Mitchell, M. -C. Fok, E. C. Roelof, and R. Demajistre, Global ENA observations of the storm mainphase ring current: Implications for skewed electric fields in the inner magnetosphere, *Geophys. Res. Lett., 29(20)*, 1954, doi:10.1029/2002GL015160, 2002.

Dessler, A. J., and R. Karplus, Some effects of diamagnetic ring currents on Van Allen radiation, *J. Geophys. Res., 66*, 2289–2295, 1961.

DeZeeuw D., A. Ridley, G. Toth, T. Gombosi, K. Powell, and R. Wolf, Inner magnetosphere simulations–Coupling the Michigan MHD model with the Rice Convection Model, *Eos. Trans. AGU, 82*(47), Fall Meet. Suppl., Abstract SM42A-0830, 2001.

Elkington, S. R., M. K. Hudson, and A. A. Chan, Acceleration of relativistic electrons via drift-resonant interaction with toroidal-mode Pc-5 ULF oscillations, *Geophys. Res. Lett., 26*, 3273–3276, 1999.

Fok, M.-C., and T. E. Moore, Ring current modeling in a realistic magnetic field configuration, *Geophys. Res. Lett.*, *24*, 1775–1778, 1997.

Fok, M.-C., J. U. Kozyra, A. F. Nagy, and T. E. Cravens, Lifetime of ring current particles due to Coulomb collisions in the plasmasphere, *J. Geophys. Res.*, *96*, 7861–7867, 1991.

Fok, M.-C., J. U. Kozyra, A. F. Nagy, C. E. Rasmussen, and G. V. Khazanov, Decay of equatorial ring current ions and associated aeronomical consequences, *J. Geophys. Res.*, *98*, 19381–19393, 1993.

Fok, M.-C., P. D. Craven, T. E. Moore, and P. G. Richards, Ring current—plasmasphere coupling through Coulomb collisions, in *Cross-Scale Coupling in Space Plasmas, Geophys. Monogr. Ser., vol. 93*, edited by J. L. Horwitz, N. Singh, and J. L. Burch, pp. 161–171, AGU, Washington, D. C., 1995.

Fok, M.-C., T. E. Moore, and M. E. Greenspan, Ring current development during storm main phase, *J. Geophys. Res.*, *101*, 15,311–15,322, 1996.

Fok, M.-C., T. E. Moore, and W. N. Spjeldvik, Rapid enhancement of radiation belt electron fluxes due to substorm dipolarization of the geomagnetic field, *J. Geophys. Res., 106,* 3873–3881, 2001a.

Fok, M.-C., R. A. Wolf, R. W. Spiro, and T. E. Moore, Comprehensive computational model of the Earth's ring current, *J. Geophys. Res., 106*, 8417–8424, 2001b.

Fok, M.-C., T. E. Moore, G. R. Wilson, J. D. Perez, X. X. Zhang, P. C:son Brandt, D. G. Mitchell, E. C. Roelof, J.-M. Jahn, C. J. Pollock, and R. A. Wolf, Global ENA IMAGE simulations, *Space Sci. Rev.*, *109*, 77–103, 2003.

Foster, J. C. and H. B. Vo, Average characteristics and activity dependence of the subauroral polarization stream, *J. Geophys. Res, 107*(A12), 1475, doi: 10.1029/2002JA009409, 2002.

Gombosi, T. I., D. L. DeZeeuw, K. G. Powell, A. J. Ridley, I. V. Sokolov, Q. F. Stout, and G. Toth, Adaptive mesh refinement for global magnetohydrodynamic simulation, in *Space Plasma Simulation*, edited by J. Buchner, C. T. Dum, and M. Scholer, pp. 247–274, Springer-Verlag Berlin Heidelberg, 2003.

Groth, C. P. T., D. L. Zeeuw, T. I. Gombosi, and K. G. Powell, Global three-dimensional MHD simulation of a space weather event: CME formation, interplanetary propagation, and interaction with the magnetosphere, *J. Geophys. Res., 105*, 25053–25078, 2000.

Hardy, D. A., M. S. Gussenhoven, R. Raistrick, and W. J. McNeil, Statistical and functional representations of the pattern of auroral energy flux, number flux, and conductivity, *J. Geophys. Res., 92*, 12,275–12,294, 1987.

Harel, M., R. A. Wolf, P. H. Reiff, R. W. Spiro, W. J. Burke, F. J. Rich, and M. Smiddy, Quantitative simulation of a magnetospheric substorm, 1, Model logic and overview, *J. Geophys. Res., 86*, 2217–2241, 1981.

Hedin, A. E., Extension of the MSIS thermospheric model into the middle and lower atmosphere, *J. Geophys. Res.*, *96*, 1159–1172, 1991.

Horne R. B., N. P. Meredith, R, M Thorne, D. Heynderickx, R. H. A. Iles, and R. R. Anderson, Evolution of energetic electron pitch angle distributions during storm time electron acceleration to MeV energies, *J. Geophys. Res., 108*(A1), 1016, 2003.

Hudson, M. K., S. R. Elkington, J. G. Lyon, V. A. Marchenko, I. Roth, M. Temerin, and M. S. Gussenhoven, MHD/particle simulations of radiation belt formation during a storm sudden commencement, in *Radiation Belts: Models and Standards*, *Geophys. Monogr. Ser.*, vol. 97, edited by J. F. Lemaire, D. Heynderickx, and D. N. Baker, pp. 57–62, AGU, Washington, D. C., 1996.

Jordanova, V. K., J. U. Kozyra, A. F. Nagy, and G. V. Khazanov, Kinetic model of the ring current-atmosphere interactions, *J. Geophys. Res.*, *102*, 14,279–14,291, 1997.

Jordanova, V. K., C. J. Farrugia, R. M. Thorne, G. V. Khazanov, G. D. Reeves, and M. F. Thomsen, Modeling ring current proton precipitation by electromagnetic ion cyclotron waves during the May 14–16, 1997, storm, *J. Geophys. Res., 106*, 7–22, 2001.

Kennel, C. F., and H. E. Petsheck, Limit on stably trapped particles fluxes, *J. Geophys. Res., 71*, 1, 1966.

Khazanov, G. V., M. W. Liemohn, T. S. Newman, M.-C. Fok, and R. W. Spiro, Self-consistent magnetosphere-ionosphere coupling: Theoretical studies, *J. Geophys. Res., 108*(A3), 1122, doi:10.1029/2002JA009624, 2003a.

Khazanov, G. V., K. V. Gamayunov, and V. K. Jordanova, Self-consistent model of magnetospheric ring current and electromagnetic ion cyclotron waves: The 2–7 May 1998 storm, *J. Geophys. Res., 108*(A12), 1419, doi:10.1029/2003JA009856, 2003b.

Kim, H.-J., and A. A. Chan, Fully relativistic changes in storm time relativistic electron fluxes, *J. Geophys. Res., 102*, 22107–22116, 1997.

Kozyra, J. U., M.-C. Fok, E. R. Sanchez, D. S. Evans, D. C. Hamilton, and A. F. Nagy, The role of precipitation losses in producing the rapid early recovery phase of the Great Magnetic Storm of February 1986, *J. Geophys. Res.*, *103*, 6801–6814, 1998.

Le, G., C. T. Russell, and K. Takahashi, Morphology of the ring current derived from magnetic field observations, *Ann. Geophys., 22*, 1267–1295, 2004.

Liemohm, M. W., A. J. Ridley, D. L. Gallagher, D. M. Ober, and J. U. Kozyra, Dependence of plasmaspheric morphology on the electric field description during the recovery phase of the 17 April 2002 magnetic storm, *J. Geophys. Res., 109*, A03209, 2004.

Lyons, L. R., and D. J. Williams, *Quantitative Aspects of Magnetospheric Physics*, D. Reidel, Norwell, Mass. 1984.

Lyons, L. R., R. M. Thorne, and C. F. Kennel, Pitch-angle diffusion of radiation belt electrons with the plasmasphere, *J. Geophys. Res., 77*, 3455–3474, 1972.

Ober, D. M., J. L. Horwitz, and D. L. Gallagher, Formation of density troughs embedded in the outer plasmasphere by subauroral ion drift events, *J. Geophys. Res., 102*, 14,595–14,602, 1997.

Rasmussen, C. E., S. M. Guiter, and S. G. Thomas, Two-dimensional model of the plasmasphere: refilling time constants, *Planet. Space Sci.*, *41*, 35–43, 1993.

Riley, P., Electrodynamics of the low latitude ionosphere, Ph. D. thesis, Rice Univ., Houston, Tex., 1994.

Roelof, E. C., and A. J. Skinner, Extraction of distributions from magnetospheric ENA and EUV images, *Space Sci. Rev., 91*, 437–459, 2000.

Rowland, D. E., and J. R. Wygant, Dependence of the large-scale, inner magnetospheric electric field on geomagnetic activity, *J. Geophys. Res.*, *103*, 14,959–14,964, 1998.

Sandel, B. R. et al., The extreme ultraviolet imager investigation for the IMAGE mission, *Space Sci. Rev., 91*, 197–242, 2000.

Skoug, R. M. et al., A prolonged He^+ enhancement within a coronal mass injection ejection in the solar wind, *Geophys. Res. Lett., 26*, 161–164, 1999.

Summers, D., and C.-Y. Ma, A model for generating relativistic electrons in the Earth's inner magnetosphere based on gyroresonant wave-particle interactions, *J. Geophys. Res., 105*, 2625–2639, 2000.

Summers, D., R. M. Thorne, and F. Xiao, Relativistic theory of wave-particle resonant diffusion with application to electron acceleration in the magnetosphere, *J. Geophys. Res., 103*, 20,487–20,500, 1998.

Toffoletto, F., S. Sazykin, R. Spiro, and R. Wolf, Inner magnetospheric modeling with the Rice Convection Model, *Space Sci. Rev., 107*, 175–196, 2003.

Tsyganenko, N. A., Modeling the Earth's magnetospheric magnetic field confined within a realistic magnetopause, *J. Geophys. Res.*, *100*, 5599–5612, 1995.

Tsyganenko, N. A., A model of the near magnetosphere with a dawn-dusk asymmetry 2. Parameterization and fitting to observations, *J. Geophys. Res., 107* (A8), 10.1029/2001JA000220, 2002.

Walt, M, Source and loss processes for radiation belt particles, in *Radiation Belts: Models and Standards, Geophys. Monogr. Ser.,* vol. 97, edited by J. F. Lemaire et al., pp. 1–13, AGU, Washington, D. C., 1996.

Weimer, D. R., Models of high-latitude electric potentials derived with a least error fit of spherical harmonic coefficients, *J. Geophys. Res.*, *100*, 19595–19607, 1995.

Weimer, D. R., An improved model of ionospheric electric potentials including substorm perturbations and applications to the Geospace Environment Modeling November 24, 1996, event, *J. Geophys. Res., 106*, 407–416, 2001.

Wolf, R. A., The quasi-static (slow-flow) region of the magnetosphere, in *Solar Terrestrial Physics*, edited by R. L. Carovillano and J. M. Forbes, pp. 303–368, D. Reidel, Norwell, Mass., 1983.

Wolf, R. A., Magnetospheric Configuration, in *Introduction to Space Physics*, edited by M. G. Kivelson and C. T, Russell, chap. 10, Cambridge University Press, New York, 1995.

Zheng, Y., M.-C. Fok, and G. V. Khazanov, A radiation belt—ring current forecasting model, *Space Weather*, *1*(3), 1013, 2003.

Y. Ebihara, National Institute of Polar Research, 1-9-10 Kaga, Itabashi-ku, Tokyo 173-8515, Japan.

M.-C. Fok, and T. E. Moore, NASA Goddard Space Flight Center, Code 612.2, Greenbelt, MD 20771, USA.

K. A. Keller, S P System, NASA Goddard Space Flight Center, Code 612.3, Greenbelt, MD 20771, USA.

D. M. Ober, Mission Research Corporation, 589 West Hollis Street Suite 201, Nashua, NH 03062, USA